Entanglement distillation by adiabatic passage in coupled quantum dots

Jaroslav Fabian and Ulrich Hohenester
Institute of Physics, Karl-Franzens University, Universitätsplatz 5, 8010 Graz, Austria

Adiabatic passage of two correlated electrons in three coupled quantum dots is shown to provide a robust and controlled way of distilling, transporting and detecting spin entanglement, as well as of measuring the rate of spin disentanglement. Employing tunable interdot coupling the scheme creates, from an unentangled two-electron state, a superposition of spatially separated singlet and triplet states. A single measurement of a dot population (charge) collapses the wave function to either of these states, realizing entanglement to charge conversion. The scheme is robust, with the efficiency close to 100%, for a large range of realistic spectral parameters.

PACS numbers: 03.67.Mn, 03.67.Hk, 03.67.Lx, 73.63.Kv

Creation and detection of spin entanglement is a major task for quantum information processing[1]. A particular implementation of the processing relies on electron spins in coupled quantum dots, proposed as qubits for quantum inverters [2] and for universal gating in quantum computation [3]. It has been proposed that entangled two-electron spin states in quantum dots can be produced by tuned quantum gates [3–5], by filtering through time-dependent barriers [6], or by projective measurements [7, 8]. Entanglement is proposed to be detected by current noise measurements [9]. Impressive recent progress in coherent control of electronic states in quantum dots [10–13] and spin coherence [14] gives strong impetus to these concepts.

Here we introduce a scheme for performing spin entanglement distillation. The remarkable feature of the scheme is that, unlike previous proposals, it is also capable of entanglement detection, transport, as well as disentanglement measurement, all in a robust way, without the need for fine tuning or precise knowledge of spectral or pulse parameters. The scheme is based on our finding of a strong correlation between adiabatic passage and entanglement: a single adiabatic pulse induces entirely different adiabatic passages of different Bell (maximally entangled) spin states. We call our scheme, which can be realized by current experimental techniques, entanglement distillation by adiabatic passage (EDAP).

We demonstrate the scheme on two electrons in three coupled quantum dots. Starting from an unentangled pair, a combination of temporal pulse sequences of interdot couplings spatially separates singlet and triplet states. Entanglement is converted to charge whose detection uniquely gives a triplet or a singlet. The same principle is used for entanglement detection. The scheme transports triplets only, leaving singlets, allowing for selective transport of entangled pairs. Our work is motivated by quantum control techniques for atomic systems such as adiabatic passage and stimulated Raman adiabatic passage (STIRAP) [15] which are increasingly used in solid state physics [16, 17]. For example, STIRAP has been recently proposed to transport single electrons [18], and adiabatic passage to spatially separate electron singlet pairs[19], in coupled dots.

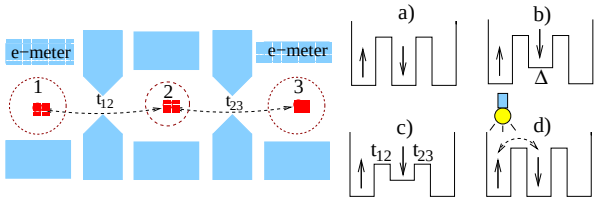

FIG. 1: Entanglement distillation by adiabatic passage. Three quantum dots are coupled via electrode-defined barriers giving tunnel couplings t_{12} and t_{23}. The ground state energy of dot 2 is shifted by Δ. The charge on dots 1 or 3 is detected by electrometers. On the right the four figures show the scheme at work [the light bulb in d) is an electrometer]

We model the physics of two electrons in three coupled dots (Fig. 1) by the time-dependent Hubbard Hamiltonian

$$H = \sum_{i\lambda} \varepsilon_i n_{i\lambda} + \sum_{i<j,\lambda\lambda'} U_{i\lambda,j\lambda'} n_{i\lambda} n_{j\lambda'} + \sum_{ij,\lambda} t_{ij} a^+_{i\lambda} a_{j\lambda}, \quad (1)$$

with the Fermi creation ($a^+_{i\lambda}$) and annihilation ($a_{i\lambda}$) operators for dot i (1, 2, and 3) and spin $\lambda =\uparrow,\downarrow$, and number operators $n_{i\lambda} = a^+_{i\lambda} a_{i\lambda}$. The confining energies ε_i do not depend on spin. We take $\varepsilon_1 = \varepsilon_3 = 0$, while setting an offset for the middle dot $\varepsilon_2 = \Delta$. The offset can be controlled electrostatically, or it can be fixed within a useful spectral range as shown below. We take the on-site Coulomb repulsion $U_{i\uparrow,i\downarrow} = U$ to be the same for all dots; similarly for the off-site interactions $U_{i,\lambda;i+1,\lambda'} = V$, and zero otherwise. Hopping integrals representing interdot couplings are t_{ij}. For our system only t_{12} and t_{23} are not zero and depend on time t, so that $H = H(t)$. The interdot couplings are modulated by electrostatic gates defining interdot barriers. The spectral scales are meVs, with $t \ll U$ for realistic systems. In the examples below we use generic values of $U = 1$ meV, $V = 0$ or 0.1 meV, and maximum hoppings smaller than 0.1 meV. Precise values will not be relevant.

The time dependent spectrum of H, in the presence of interdot coupling pulses, is shown in Fig. 2a. We

take Gaussian pulses of the form $t_{ij}(t) = t_0 \exp(t^2/2\tau^2)$, where t_0 is the maximum pulse strength and τ is the dispersion. The overlap between the pulses is taken to be 2τ, the width of one pulse. There are three weakly coupled groups of states. The lowest states with energy $E \approx 0$ consist of electrons occupying mainly dots 1 and 3. The highest state, of $E \approx U + 2\Delta$, is for a double occupancy of dot 2. The states relevant for EDAP have $E \approx U, \Delta$, and comprise electron singlets and triplets on neighboring dots. These states are magnified in Fig. 2b. To simplify notation we introduce the following labels for triplet T and singlet S states on dots i and j (assuming $i < j$), as well as for double occupancy states D:

$$|T_1\rangle_{ij} = a^+_{i\uparrow}a^+_{j\uparrow}|0\rangle, \quad |T_{-1}\rangle_{ij} = a^+_{i\downarrow}a^+_{j\downarrow}|0\rangle, \tag{2}$$

$$|T_0\rangle_{ij} = (1/\sqrt{2})(a^+_{i\uparrow}a^+_{j\downarrow} + a^+_{j\uparrow}a^+_{i\downarrow})|0\rangle, \tag{3}$$

$$|S\rangle_{ij} = (1/\sqrt{2})a^+_{i\uparrow}a^+_{j\downarrow} - a^+_{j\uparrow}a^+_{i\downarrow}|0\rangle, \tag{4}$$

$$|D\rangle_i = a^+_{i\uparrow}a^+_{i\downarrow}|0\rangle. \tag{5}$$

Here $|0\rangle$ is the vacuum. The triplet states $|T_{S_z}\rangle$ are labeled by their spin S_z. States $|T_0\rangle$ and $|S\rangle$ are spin entangled.

We first summarize EDAP steps and then discuss the physics in detail. The scheme is shown in Fig. 1: (a) Start with two uncoupled electrons occupying neighboring dots 1 and 2. (b) Raise slowly the energy of the middle dot 2 to Δ being on the scale of U (this step is not necessary if Δ is built in). (c) Apply an overlapping pulse sequence of t_{12} and t_{23} (order not relevant). After the pulses fade away, Δ can be switched back to zero, if necessary. The resulting state is with a high probability a superposition of a singlet state, spread over dots 1 and 2, and triplet states, on dots 2 and 3. A detection of (the absence of) charge in dot 1, collapses the wave function to the singlet (triplet). Mathematically, an initial two-electron state $\Psi(t = 0)$ localized on dots 1 and 2, is a superposition

$$\Psi(0) = a|S\rangle_{12} + b|T_0\rangle_{12} + c|T_1\rangle_{12} + d|T_{-1}\rangle_{12}. \tag{6}$$

After EDAP, the state will be

$$\Psi(\infty) = a'|S\rangle_{12} + b'|T_0\rangle_{23} + c'|T_1\rangle_{23} + d'|T_{-1}\rangle_{23}, \tag{7}$$

where the primed coefficients are equal to unprimed up to a phase factor. The singlet state returns to the initial dots while the triplets are transported to dots 2 and 3. As a result entanglement is coupled to charge on dots 1 and 3. The scheme also works as a noninvasive entanglement detector. If the initial state is a singlet, the final state is the same (up to a phase). If it is a triplet, the state is shifted in space. Charge measurement on dots 1 or 3, which is a nondemolition measurement for singlet and triplet states in the absence of interdot coupling, separates the two. In general, probabilities of finding, say the singlet in a given initial state, $|a|^2$ can be obtained by repeating the measurement on the identically prepared state, detecting a degree of entanglement. The scheme does not, however, discern the individual triplet states $|T_0\rangle$ and $|T_{\pm1}\rangle$ without an additional single-dot control (e.g., spin rotation). Finally, the scheme detects disentanglement and charge decoherence by observing systematic deviations from the expected final states (e.g., detecting charge on *both* 1 and 3).

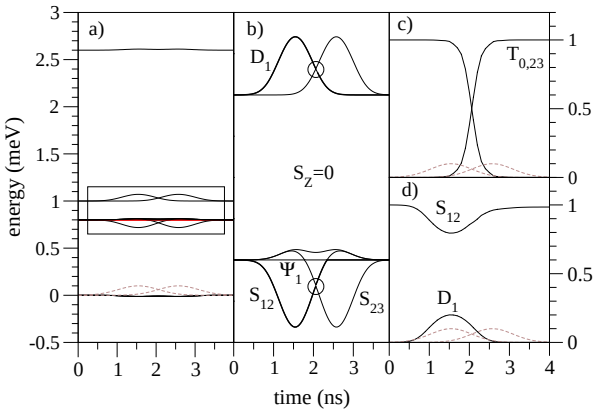

FIG. 2: (a) Temporal evolution of the two-electron spectrum (solid lines) of Hamiltonian H in the presence of two overlapping Gaussian pulses (dashed) of t_{12} and t_{23}. The spectra are plotted for $U = 1$ meV, $V = 0$, and $\Delta = 0.8$ meV. The pulses of $t_{12}(t)$ and $t_{23}(t)$ have widths $\tau \approx 500$ ps. (b) States with $S_z = 0$ relevant for EDAP, from the box in a). There is a level repulsion (anticrossing) inside the circles, where the passage is rapid. At other two crossings there is no repulsion. The horizontal line is the trapped state Ψ_1. (c) Counterintuitive passage scheme for Ψ_1 showing probabilities p of finding states $|T_0\rangle_{12}$ and $|T_0\rangle_{23}$. (d) Passage scheme for $|S\rangle_{12}$ showing the probabilities p of observing $|S\rangle_{12}$ and $|D_1\rangle$.

To demonstrate the scheme we study the evolution of each of the states in the superposition of Eq. (6). Consider triplet states first. It is useful to find the eigenstates of H whose energies do not depend on t_{12} or t_{23}; in analogy with quantum optics, we call these states trapped. There are four two-electron trapped states of H:

$$\Psi_1 = \sin\varphi|T_0\rangle_{12} - \cos\varphi|T_0\rangle_{23}, \tag{8}$$

$$\Psi_2 = \sin\varphi|T_1\rangle_{12} - \cos\varphi|T_1\rangle_{23}, \tag{9}$$

$$\Psi_3 = \sin\varphi|T_{-1}\rangle_{12} - \cos\varphi|T_{-1}\rangle_{23}, \tag{10}$$

$$\Psi_4 = [|D\rangle_1 - |D\rangle_2 + |D\rangle_3]/\sqrt{3}. \tag{11}$$

The mixing angle $\varphi = \varphi(t)$ is defined by $\tan\varphi = t_{12}/t_{23}$. States Ψ_1 through Ψ_3 have energy $V+\Delta$, while Ψ_4, which is trapped only for $\Delta = 0$, has energy U. As in STIRAP, which is a technique for population transfer via trapped states[15], states Ψ_1 through Ψ_3 allow the passage of an initial triplet state $|T\rangle_{12}$ to $|T\rangle_{23}$, or vice versa. Take Ψ_1 a an example. If the initial state is $|T_0\rangle_{12}$, it will be 100% in Ψ_1 for $t_{23} = 0$, when t_{12} is slowly turned on ($\varphi = \pi/2$). The state is unaltered until a subsequent overlapping pulse of t_{23} will smoothly move the state to

$\Psi_1 = |T_0\rangle_{23}$, after t_{12} vanishes ($\varphi = 0$). During the passage, no state other than the two triplets is populated. The numerical calculation is shown in Fig. 2c, confirming the qualitative picture. In our context this pulse sequence (t_{12} before t_{23}) can be called counterintuitive, while the opposite order (t_{23} before t_{12}) intuitive. Transfer through Ψ_1 by counterintuitive sequence is extremely robust, independent on spectral parameters, as long as adiabatic conditions, to be specified, hold. While adiabatic passage via Ψ_1 is a nine-level process (there are nine $S_z = 0$ basis states), the scheme with Ψ_2 and Ψ_3, for transporting spin unentangled triplets $|T_1\rangle$ and $|T_{-1}\rangle$, is an exact analogue of the three level STIRAP. Triplet states can also be transferred through intuitive sequencing (not via Ψ_1), if Δ is greater than the interdot couplings. Such a transfer is less robust, but for our scheme it is equally satisfactory as counterintuitive, since we need $\Delta \gtrsim t_{12}, t_{23}$ to transfer singlet states, as shown below. The fourth trapped state, Ψ_4, is a superposition of doubly occupied states. Because it cannot be manipulated with interdot couplings, we call this state globally trapped. We will not use this state below.

Singlet states are not part of the trapped states. If the initial state is the singlet $|S\rangle_{12}$, the above scheme in general leads to an arbitrary superposition of eigenstates of H for isolated dots. There is, however, a window of energy offsets Δ where the final state will be $|S\rangle_{12}$, up to a phase. Consider states $|S\rangle_{12}$, $|D\rangle_1$, and $|D\rangle_2$, with average energies $\Delta + V$, U, and $2\Delta + U$, respectively. If we make Δ on the same scale as U, state $|D\rangle_2$, as well as all other eigenstates, will not be easily accessible due to spectral separation (Fig. 2a). We have an effective two-level system with Hamiltonian (up to a constant)

$$H' = \frac{1}{2}(\Delta + V - U)\sigma_z + \sqrt{2}t_{12}(t)\sigma_x, \qquad (12)$$

where σ_α are the Pauli matrices. The eigenstates are

$$\Psi_+ = \cos(\vartheta/2)\,|S\rangle_{12} + \sin(\vartheta/2)\,|D\rangle_1, \qquad (13)$$
$$\Psi_- = \sin(\vartheta/2)\,|S\rangle_{12} - \cos(\vartheta/2)\,|D\rangle_1. \qquad (14)$$

The mixing angle $\vartheta = \vartheta(t)$, restricted to $[0, \pi]$, is defined by $\tan\vartheta = 2\sqrt{2}t_{12}/(\Delta + V - U)$. The nature of the time evolution of the singlet depends critically on Δ. In resonance, $\Delta + V \approx U$, the singlet is initially a superposition of Ψ_+ and Ψ_-. After passage of pulse t_{12} the final state will be $\Psi(\infty) = |S\rangle_{12}\cos\alpha + |D\rangle_1 \sin\alpha$, where the pulse area $\alpha = \int \sqrt{2}t_{12}(t)dt$. By fine tuning the pulses to $\alpha = \pi$, the final state will be $|S\rangle_{12}$.

The above resonant scheme for singles, though allowing fine control, is not robust: it requires both the resonance condition and precise knowledge of the pulse area. We instead explore the large spectral window off the resonance. For $|\Delta + V - U| \gtrsim t_{12}$, state $|S\rangle_{12}$ will be transported back to itself, via Ψ_+. (This is analogous to adiabatically following of a spin along a magnetic field that rotates along y-axis back and forth adiabatically.) Such a passage is very robust. The two-level picture is confirmed by the numerical calculation with the full Hamiltonian H in Fig. 2d.

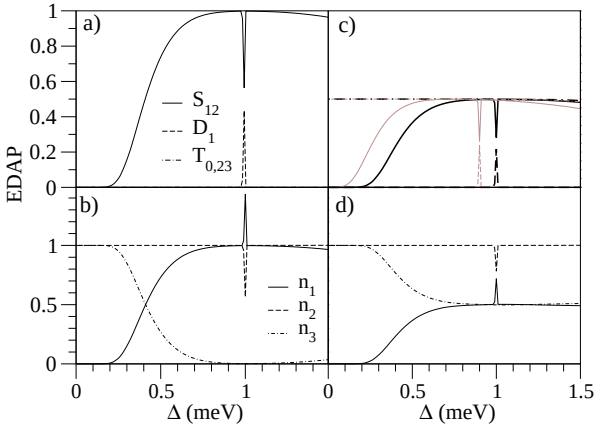

FIG. 3: a) Calculated probabilities and electron populations after EDAP passage as a function of Δ, with $\Psi(0) = |S\rangle_{12}$ (a and b) and $\Psi(0) = a^+_{1\uparrow}a^+_{2\downarrow}|0\rangle$ (c and d). The thin dotted lines in c) are for $V = 0.1$ meV. Pulses are the same as in Fig. 2.

Figure 3 shows EDAP results as a function of Δ, for two initial states. For the selected τ the initial singlet returns to the same state at least 90% of times for $\Delta \gtrsim$ 0.6 meV (unless at resonance visible by spikes). This is closely mirrored by the charge population of the dots 1 and 3. Dot 2 has always charge one, except for resonance, in which dot 1 can be doubly occupied. The influence of off-site Coulomb interaction is seen in Fig. 3c. The only effect is shifting the resonance from $\Delta = U$ to $\Delta = U - V$.

What is the condition on the pulse? Passage of state $|l\rangle$ is adiabatic if $|\langle l|\dot{\hbar H}(t)|k\rangle| \ll (\hbar\omega_{lk})^2$, where k are other eigenstates of $H(t)$ and ω_{lk} are the Bohr frequencies [20]. We give rough estimates for the limits on pulse dispersion τ (switching time), based on the qualitative criterion that the smallest relevant Bohr period needs to be resolved during the passage. EDAP comprises four processes: (i) Adiabatic passage of the triplet state. For $|\Delta| \lesssim t_0$, which can be used for triplet transport, this is robust if $\tau \gtrsim \hbar/t_0$. In our scheme $\Delta \gg t_0$ and the smallest relevant Bohr energy is t_0^2/Δ. Then $\tau \gtrsim \tau_L$ where $\tau_L = \hbar/(t_0^2/\tau)$ gives the lower limit. (ii) Adiabatic passage of the singlet. This is a two-level scheme with states separated by $\sim t_0$. Thus $\tau \gtrsim \hbar/t_0$, which is within the range of (ii) and need not be considered extra. (iii) Rapid passage of the singlet through the anticrossing at time t given by $\bar{t} = t_{12}(t) = t_{23}(t)$ (Fig. 2b). The level repulsion is small, since $|S\rangle_{12}$ couples to $|S\rangle_{23}$ through spectrally distant states such as $|S\rangle_{13}$ and $|D\rangle_2$. Interference in the virtual coupling to these states further reduces the anticrossing. One can show that the level spacing is $V_g \approx 2(\bar{t}^2/\Delta)(U - \Delta)/(U + \Delta)$, vanishingly small at resonance in the oder $O(\bar{t}^2/\Delta)$. Rapid

passage occurs for $\tau' \lesssim \hbar/V_g$, where $\tau' = \tau V_g/t_0$ is the time over which the interdot coupling changes by V_g, relevant for resolving the gap. This gives $\tau \lesssim \tau_U$ where $\tau_U = \tau_L \times (\Delta/t_0)(U+\Delta)/(U-\Delta)$ is the upper limit. Finally, (iv) EDAP has to be performed within the coherence time of the system, which is, at low temperatures, likely in the nanosecond time scale [10, 13]. Considering full coherence, the time limitations on the pulse are $\tau_L \lesssim \tau \lesssim \tau_U$, which for our model parameters is 100 ps to 10 ns. Since the lower limit is given by energy t_0^2/Δ which is on the order of the exchange coupling ($J = t_0^2/U$ in the Hubbard model) for our case of $\Delta \approx U$, the times are similar to those used for spin-based quantum computing [4]. The upper limit τ_U increases with decreasing $|U - \Delta|$. The scheme will perform quadratically faster for larger couplings.

To identify numerically the regime of applicability of the scheme, we define EDAP efficiency w as

$$w = |\langle\Psi(\infty)|S\rangle_{12}|^2 + |\langle\Psi(\infty)|T_0\rangle_{23}|^2, \qquad (15)$$

for a state $\Psi(t)$ with the initial condition $\Psi(0) = a^+_{1\uparrow}a^+_{2\downarrow}|0\rangle$. This definition is insensitive to the relative phase change, and to the relative population of the two states. The efficiency is plotted in Fig. 4 as a function of Δ and τ for the counterintuitive sequence (intuitive shows the same picture except at Δ close to 0). The range of applicability, from 100 ps to 10 ns agrees with our analytical estimates for our parameters. The graph also shows the predicted increase of applicable τ with decreasing $|U - \Delta|$. It is evident that our scheme is very robust, covering large range of spectral values and pulse times. The horizontal "cut" at $\Delta = U = 1$ meV indicates the resonance oscillations of the $|S\rangle_{12} - |D\rangle_1$ pair for which the efficiency depends on the area of the pulse, α, and thus on τ. The lower limit on τ can be further reduced by about a decade (to 50 ps for 98% efficiency for our parameters) by decreasing the delay between the pulses (not shown here).

Efficiency w can be measured by performing EDAP twice: if the first (distillation) passage results in, say, singlet, the second (detection) passage should give absence of charge on dot 3, if $w \approx 1$. Another interesting application of EDAP can be in quantifying the influence of a charge probe on the charge itself. Say, use EDAP to transport triplets via Ψ_1. Since $n_2\Psi_1 = \Psi_1$ at all times (in fact, Ψ_1 through Ψ_3 are the only eigenstates of $H(t)$ that are also eigenstates of n_2), a measurement of population on dot 2 should not disturb the state. EDAP efficiency loss is a measure of the invasiveness of the probe.

In conclusion, we have proposed a robust and realistic all-electronic scheme for distilling and detecting two-electron spin entanglement in coupled quantum dots. The scheme converts entanglement to charge, with close to 100% efficiency, by spatially separating singlet and triplet states within a single superposition. Because the entanglement detection is nondestructive the scheme can be used repetitively to transport entangled pairs as well as to detect disentanglement. Although we have used the example of quantum dots, we believe that EDAP is general enough to be applicable in other physical implementations of quantum information processing.

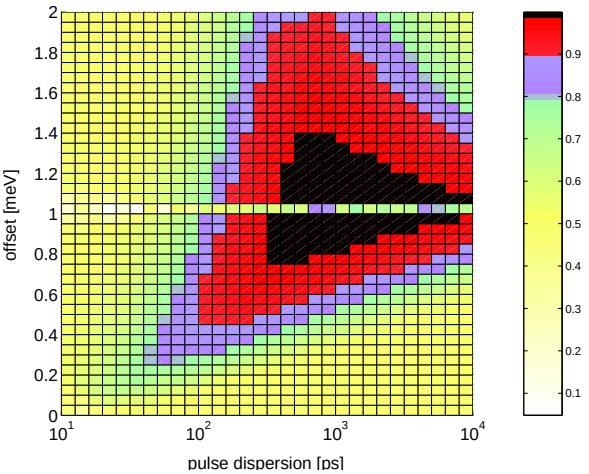

FIG. 4: Calculated efficiency w as a function of the pulse dispersion τ and offset Δ, for the counterintuitive pulse sequence. The darkest window is for efficiency higher than 98%, while the second darkest (red) one is for $w > 90\%$.

This work was supported by the US ONR and FWF.

[1] C. H. Bennett and D. P. DiVincenzo, *Nature* **404**, 247 (2000).
[2] S. Bandyopadhyay and V. P. Roychowdhury, Superlattices Microstruct. **22**, 411 (1997).
[3] D. Loss and D. P. DiVincenzo, Phys. Rev. A **57**, 120 (1998).
[4] G. Burkard, D. Loss, and D. P. DiVincenzo, Phys. Rev. B **59**, 2070 (1999).
[5] X. Hu and S. Das Sarma, Phys. Rev. A **61**, 062301 (2000).
[6] X. Hu and S. Das Sarma, Phys. Rev. B **69**, 115312 (2004).
[7] R. Ruskov and A. N. Korotkov, Phys. Rev. B **67**, 241305(R) (2003).
[8] T. M. Stace, S. D. Barrett, H. S. Goan, and G. J. Milburn (2004), cond-mat/0410181.
[9] D. Loss and E. V. Sukhorukov, Phys. Rev. Lett. **84**, 1035 (2000).
[10] J. R. Petta, A. C. Johnson, C. M. Marcus, M. P. Hanson, and A. C. Gossard, Phys. Rev. Lett. **93**, 186802 (2004).
[11] T. Hayashi, T. Fujisawa, H. D. Cheong, Y. H. Jeong, and Y. Hirayama, Phys. Rev. Lett. **91**, 226804 (2003).
[12] W. G. van der Wiel, S. De Franceschi, J. M. Elzerman, T. Fujisawa, S. Tarucha, and L. P. Kouwenhoven, Rev. Mod. Phys. **75**, 1 (2003).
[13] J. R. Petta, A. C. Johnson, A. Jacoby, C. M. Marcus, M. P. Hanson, and A. C. Gossard (2004), cond-mat/0412048.
[14] R. Hanson, B. Witkamp, L. M. K. Vandersypen, L. H.

Willems van Beveren, J. M. Elzerman, and L. P. Kouwenhoven, Phys. Rev. Lett. **91**, 196802 (2003).
[15] K. Bergmann, H. Theuer, and B. W. Shore, Rev. Mod. Phys. **70**, 1003 (1998).
[16] T. Brandes (2004), cond-mat/0409771.
[17] U. Hohenester (2004), cond-mat/0406346.
[18] A. D. Greentree, J. H. Cole, A. R. Hamilton, and L. C. L. Hollenberg (2004), cond-mat/0407008.
[19] P. Zhang, Q. K. Xue, X. G. Zhao, and X. C. Xie, Phys. Rev. A **69**, 042307 (2004).
[20] A. Messiah, *Quantum Mechanics*, vol. II (North-Holland, Amsterdam, 1965).